Inorganic Chemistry
Article

Inorg. Chem. 2010, 49, 7545–7548 7545
DOI: 10.1021/ic101022f

Theoretical Analysis of the Spin Exchange and Magnetic Dipole−Dipole Interactions Leading to the Magnetic Structure of Ni_3TeO_6

Fang Wu,[†,‡] Erjun Kan,[‡] Chuan Tian,[‡] and Myung-Hwan Whangbo*[,‡]

[†]*School of Science, Nanjing Forestry University, Nanjing, Jiangsu 210037, People's Republic of China, and*
[‡]*Department of Chemistry, North Carolina State University, Raleigh, North Carolina 27695-8204*

Received May 20, 2010

The origin of the collinear antiferromagnetic magnetic structure of Ni_3TeO_6 below 52 K was analyzed by calculating its spin exchanges on the basis of density functional calculations, and the cause for the $\|c$-spin orientation found for this magnetic structure by calculating the spin−orbit coupling and magnetic dipole−dipole interaction energies. The calculated exchanges correctly predict the observed magnetic structure below 52 K, and lead practically to no spin frustration. The $\perp c$- and $\|c$-spin orientations are predicted by the spin−orbit coupling and the magnetic dipole−dipole interactions, respectively. However, the magnetic dipole−dipole interactions are stronger than the spin−orbit coupling interactions, and hence are responsible for the spin orientation observed for Ni_3TeO_6.

1. Introduction

The magnetic oxide Ni_3TeO_6, crystallizing in a noncentrosymmetric space group $R3$, has the Te^{6+} and Ni^{2+} (d^8, $S = 1$) ions located at octahedral pockets of O^{2-} ions leading to three nonequivalent Ni sites (i.e., Ni1, Ni2, and Ni3).[1−3] The Ni1 and Ni2 sites form a slightly corrugated honeycomb net parallel to the ab-plane while the Ni3 sites form a trigonal net parallel to the ab-plane, and the honeycomb nets alternate with the trigonal nets along the c-direction (Figure 1a). The magnetic properties of Ni_3TeO_6, first reported nearly four decades ago, showed that its dominant spin exchange interaction is antiferromagnetic (AFM)[4] but have received little attention until the recent study of Živković et al.,[5] who carried out magnetic susceptibility, neutron diffraction, and dielectric-constant measurements for Ni_3TeO_6 because it might be a multiferroic. Their study showed that Ni_3TeO_6 exhibits no signature of ferroelectricity but undergoes a three-dimensional (3D) AFM ordering at 52 K with Curie−Weiss temperature $\theta = -56.1$ K. Below the Néel temperature $T_N = 52$ K, the Ni^{2+} moments are aligned along the c-direction and are ferromagnetically coupled within each honeycomb net of Ni1 and Ni2 spins parallel to the ab-plane. These ferromagnetic (FM) honeycomb nets repeat antiferromagnetically along the c-direction (Figure 1b)[5] such that each trigonal net of Ni3 spins has an FM coupling with the honeycomb net of Ni1 and Ni2 spins lying above but has an AFM coupling with that lying below. In this ordered magnetic state below T_N, the spins are oriented along the c-direction. In the present work we explore why Ni_3TeO_6 adopts such a magnetic structure below T_N. For this purpose, we evaluate the spin exchange interactions of Ni_3TeO_6 by employing the mapping analysis based on density functional electronic structure calculations and examine the spin orientation of the observed magnetic state below T_N in terms of spin−orbit coupling (SOC) and magnetic dipole−dipole (MDD) interactions.[6] Results of our analyses are presented in what follows.

2. Spin Exchange Paths and Calculations

In understanding the magnetic structure of Ni_3TeO_6, it is crucial to examine its local structures and hence its spin exchange paths. The Ni^{2+} and Te^{6+} ions of Ni_3TeO_6 form NiO_6 and TeO_6 octahedra. The $Ni2O_6$ and $Ni3O_6$ octahedra form face-sharing dimers with their 3-fold rotational axis along the c-direction, and so do the $Ni1O_6$ and TeO_6 octahedra (Figure 2a). The resulting $Ni2Ni3O_9$ and $Ni1TeO_9$ dimers share their edges to form two kinds of honeycomb layers of edge-sharing octahedra parallel to the ab-plane. One honeycomb layer consists of $Ni1O_6$ and $Ni2O_6$ octahedra (Figure 2b), in which the center of each hexagonal ring of edge-sharing $Ni1O_6$ and $Ni2O_6$ octahedra is capped by Ni3 on one surface and by Te on the other surface (Figure 2a,b). The other honeycomb layer consists of $Ni3O_6$ and TeO_6 octahedra (Figure 2c), in which the center of each hexagonal ring of edge-sharing $Ni3O_6$ and TeO_6 octahedra is capped by Ni1 on one surface and by Ni2 on the other surface

*To whom correspondence should be addressed. E-mail: mike_whangbo@ncsu.edu.

(1) Newnham, R. E.; Meagher, E. P. *Mater. Res. Bull.* **1967**, *2*, 549.
(2) Blasse, G.; Hordijk, W. *J. Solid State Chem.* **1972**, *5*, 395.
(3) Becker, R.; Berger, H. *Acta Crystallogr., Sect. E* **2006**, *62*, i222.
(4) Zupan, J.; Kolar, D.; Urbanc, V. *Mater. Res. Bull.* **1971**, *6*, 1353.
(5) Živković, I.; Prša, K.; Zaharko, O.; Berger, H. *J. Phys.: Condens. Matter* **2010**, *22*, 056002.
(6) Koo, H.-J.; Xiang, H. J.; Lee, C.; Whangbo, M.-H. *Inorg. Chem.* **2009**, *48*, 9051.

Published on Web 07/23/2010

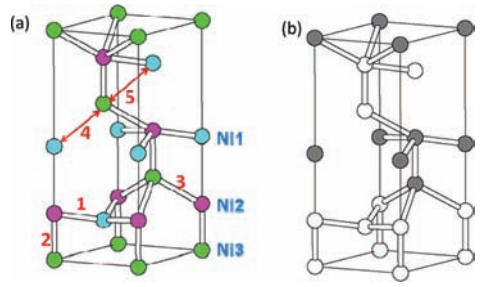

Figure 1. (a) Perspective view of the Ni^{2+} ($S = 1$) ion arrangement in Ni_3TeO_6, where the numbers 1−5 between the Ni^{2+} ($S = 1$) ions refer to the spin exchanges J_1−J_5, respectively. The Ni1 and Ni2 atoms form a slightly corrugated honeycomb net parallel to the ab-plane, while the Ni3 atoms form a trigonal net parallel to the ab-plane. (b) The spin arrangement in the magnetic ground state of Ni_3TeO_6 below T_N, where the unshaded and shaded circles represent the Ni^{2+} ($S = 1$) with down-spin and up-spin, respectively.

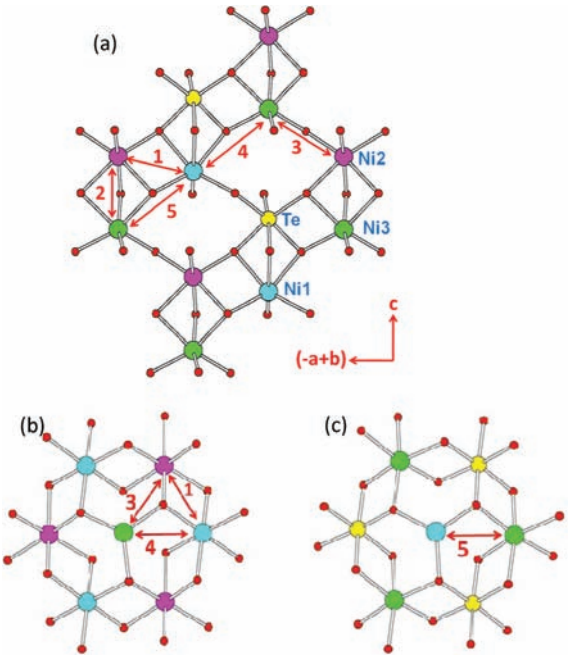

Figure 2. Structural features of Ni_3TeO_6: (a) A cross-section view of how the $Ni1O_6$, $Ni2O_6$, $Ni3O_6$, and TeO_6 octahedra are joined together. (b) A hexagonal ring of edge-sharing $Ni1O_6$ and $Ni2O_6$ octahedra, which is a part of the honeycomb layer of $Ni1O_6$ and $Ni2O_6$ octahedra. The three oxygen atoms at the center of the ring are capped with Ni3 on one surface of the ring. (c) A hexagonal ring of edge-sharing $Ni3O_6$ and TeO_6 octahedra, which is a part of the honeycomb layer of $Ni3O_6$ and TeO_6 octahedra. The three oxygen atoms at the center of the ring are capped with Ni1 on one surface of the ring. The numbers 1−5 between the Ni^{2+} ($S = 1$) ions refer to the spin exchanges J_1−J_5, respectively.

(Figure 2a,c). Each layer of $Ni3O_6$ octahedra lies in between two adjacent honeycomb layers of $Ni1O_6$ and $Ni2O_6$ octahedra such that every $Ni3O_6$ octahedron face-shares with one $Ni2O_6$ octahedron of one honeycomb layer lying above, but corner-shares with three $Ni1O_6$ and three $Ni2O_6$ octahedra of the other honeycomb layer lying below (Figure 2a,b). There are five different Ni−O−Ni superexchange paths J_1−J_5 to consider as depicted in Figure 2. J_1 occurs within a honeycomb net, while J_2−J_5 occur between adjacent honeycomb and trigonal nets. The geometrical parameters associated with the exchange paths J_1−J_5 are summarized in Table 1.

To determine the values of J_1−J_5, we carry out spin-polarized density functional calculations for the six ordered

Table 1. Geometrical Parameters Associated with the Exchange Paths J_1−J_5 in Ni_3TeO_6[a]

	Ni···Ni	Ni−O−Ni	∠Ni−O−Ni
J_1	3.000	2.150, 2.045	91.28
		2.039, 2.147	91.55
J_2	2.777	2.151, 2.122	81.07
		2.151, 2.122	81.07
		2.151, 2.122	81.07
J_3	3.459	2.039, 2.006	117.55
J_4	3.786	2.147, 2.006	131.44
J_5	3.684	2.122, 2.045	124.24

[a] The lengths are in Å, and the angles in degrees.

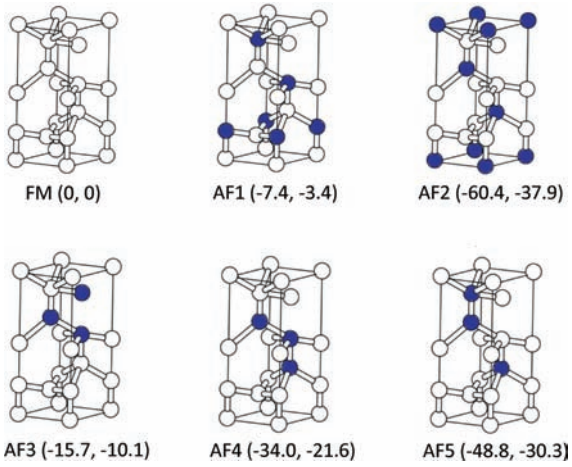

Figure 3. Six ordered spin states of Ni_3TeO_6 employed to extract the spin exchanges J_1−J_5. The unshaded and shaded circles represent the Ni^{2+} ions with up-spin and down-spin, respectively. The numbers in the parentheses for each state are the relative energies obtained from the GGA+U calculations, with the left and right numbers referring to the cases of $U = 2.5$ and 4.5 eV, respectively.

spin states of Ni_3TeO_6 (Figure 3) by using the projector augmented wave method implemented in the Vienna ab initio simulation package.[7−9] Our calculations employed the generalized gradient approximation (GGA)[10] for the exchange-correlation functional, the plane-wave cutoff energy of 400 eV, a set of 7 × 7 × 2 k-points, and the threshold 10^{-5} eV for energy convergence. To properly describe the electron correlation of the Ni 3d states, the GGA plus on-site repulsion U (GGA + U) method[11] is used with an effective U of 2.5 and 4.5 eV on the Ni atom.

To examine the spin orientation in the magnetic ground state of Ni_3TeO_6, we performed GGA+U calculations including SOC interactions. In addition, we calculated the MDD interaction energy

$$\sum_{i<J}\left(\frac{g^2\mu_B^2}{a_0^3}\right)\left(\frac{a_0}{r_{ij}}\right)^3[-3(\vec{S}_i\cdot\vec{e}_{ij})(\vec{S}_J\cdot\vec{e}_{ij})+(\vec{S}_i\cdot\vec{S}_J)] \quad (1)$$

of the magnetic ground state by considering the spins as the classical spins,[6] where $\vec{S}_i$ and $\vec{S}_j$ are the spin vectors at the

(7) Kresse, G.; Hanfner, J. *Phys. Rev. B* **1993**, *62*, 558.
(8) Kresse, G.; Furthmüller, J. *Comput. Mater. Sci.* **1996**, *6*, 15.
(9) Kresse, G.; Furthmüller, J. *Phys. Rev. B* **1996**, *54*, 11169.
(10) Perdew, J. P.; Burke, S.; Ernzerhof, M. *Phys. Rev. Lett.* **1996**, *77*, 3865.
(11) Dudarev, S. L.; Botton, G. A.; Savrasov, S. Y.; Humphreys, C. J.; Sutton, A. P. *Phys. Rev. B* **1998**, *57*, 1505.

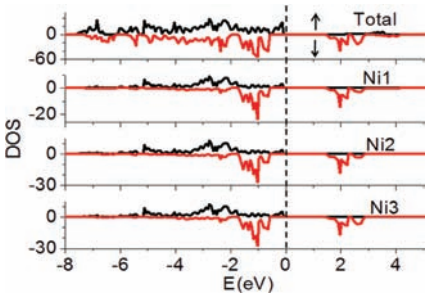

Figure 4. Plots of the total and projected DOS obtained for the FM state of Ni_3TeO_6 from the GGA+U calculations with $U = 2.5$ eV on Ni. The up-spin and down-spin states are represented by black and red curves.

spin sites i and j, respectively, g is the electron g-factor, μ_B is the Bohr magneton, a_0 is the Bohr radius (0.529177 Å), r_{ij} is the distance between the spin sites i and j, e_{ij} is the unit vector along the distance, and $(g\mu_B)^2/(a_0)^3 = 0.725$ meV.

3. Spin Exchange and Magnetic Structure

Figure 4 shows the total density of states (DOS) and the projected DOS for the Ni 3d states obtained for the FM state of Ni_3TeO_6 from the GGA+U calculations with $U = 2.5$ eV. For all the Ni1, Ni2, and Ni3 atoms, the up-spin t_{2g} and e_g states as well as the down-spin t_{2g} states are occupied while the unoccupied down-spin e_g states are separated by a band gap, which is consistent with the fact that all Ni^{2+} ions of Ni_3TeO_6 are in high-spin ($S = 1$) states. As expected, the band gap becomes greater when U is increased to 4.5 eV. Though not shown, all ordered spin states (Figure 3) employed to extract the values of J_1−J_5 have a band gap as required for magnetic insulating states.

The relative energies per formula unit (FU) of the six ordered spin states obtained from our GGA+U calculations (with $U = 2.5$ and 4.5 eV) are summarized in Figure 3. The total spin exchange interaction energies of these states can be expressed in terms of the spin Hamiltonian,

$$\hat{H} = -\sum_{i<J} J_{ij}\hat{S}_i \cdot \hat{S}_J \qquad (2)$$

defined in terms of the spin exchanges $J_{ij} = J_1$−J_5 to be determined. By applying the energy expressions obtained for spin dimers with N unpaired spins per spin site (in the present case, $N = 2$),[12,13] the total spin exchange energies per FU of the six ordered spin states are written as

$$\begin{aligned} E_{FM} &= (-9J_1 - 3J_2 - 9J_3 - 9J_4 - 9J_5)(N^2/12) \\ E_{AF1} &= (+9J_1 + 3J_2 + 9J_3 - 9J_4 - 9J_5)(N^2/12) \\ E_{AF2} &= (-9J_1 + 3J_2 + 9J_3 + 9J_4 + 9J_5)(N^2/12) \\ E_{AF3} &= (+3J_1 + J_2 - 9J_3 + 3J_4 - 9J_5)(N^2/12) \\ E_{AF4} &= (-3J_1 - J_2 - 3J_3 + 3J_1 + 3J_5)(N^2/12) \\ E_{AF5} &= (-3J_1 - J_2 + 9J_3 + 3J_1 + 3J_5)(N^2/12) \end{aligned} \qquad (3)$$

Thus, by equating the relative energies of the six ordered spin states obtained from GGA+U calculations to the corresponding relative energies obtained from the total spin exchange energies, we find the values of J_1−J_5 listed in Table 2.

(12) Dai, D.; Whangbo, M.-H. *J. Chem. Phys.* **2001**, *114*, 2887.
(13) Dai, D.; Whangbo, M.-H. *J. Chem. Phys.* **2003**, *118*, 29.

Table 2. Spin Exchange Parameters J_1−J_5 (in meV) of Ni_3TeO_6 Obtained from the GGA+U Calculations[a]

	$U = 2.5$ eV	$U = 4.5$ eV
J_1	0.94 (−0.15)	0.59 (−0.14)
J_2	4.55 (−0.71)	3.13 (−0.75)
J_3	−3.70 (0.56)	−2.19 (0.53)
J_4	−6.41 (1.00)	−4.17 (1.00)
J_5	−1.48 (0.23)	−1.01 (0.24)

[a] The numbers in the parentheses are relative values.

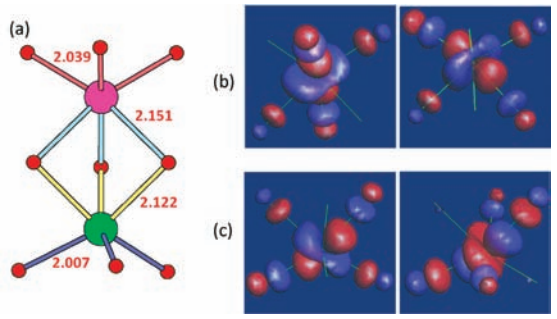

Figure 5. (a) An isolated $Ni2Ni3O_9$ face-sharing dimer, where different Ni−O bonds are indicated by the Ni−O bonds with different colors and the numbers represent the Ni−O bond lengths in Å. (b) Shapes of the two magnetic orbitals of an isolated $Ni2O_6$ octahedron. (c) Shapes of the two magnetic orbitals of an isolated $Ni3O_6$ octahedron. The orientations of the $Ni2Ni3O_9$ dimer in (b) and (c) are the same as that in (a).

Our calculations show that J_1 and J_2 are FM but J_3−J_5 are AFM. This finding is consistent with the signs of J_1−J_4 suggested on the basis of the observed magnetic structure.[5]

The exchanges J_3 are J_4 are strongly AFM, and the exchange J_2 is strongly FM. The exchange J_1 is weakly FM, while the exchange J_5 is weakly AFM. These exchanges correctly predict the observed magnetic structure below T_N. In terms of the exchanges J_1−J_5 obtained from GGA+U calculations with $U = 2.5$ and 4.5 eV, the observed magnetic structure below T_N (Figure.2b) is predicted to be more stable by 0.22 and 0.20 meV per FU, respectively, than the most stable state, AF2, of the six ordered spin states used to extract their values.

Between adjacent honeycomb and trigonal nets, there is no spin frustration in the (J_1, J_3, J_4) triangles but some spin frustration in the (J_1, J_2, J_5) triangles.[14,15] However, the latter should be negligible because J_1 and J_5 are weak. This explains why T_N and θ are nearly comparable in magnitude in Ni_3TeO_6. A magnetic compound is regarded as spin frustrated when the ratio $f = |\theta|/T_N$ is greater than 6.[14] In general, the strength of an M−O−M superexchange between two transition-metal atoms M depends on the ∠M−O−M angle and the M−O bond length.[16] The exchange J_4 is most strongly AFM, which is understandable because J_4 has a much greater ∠Ni−O−Ni angle than do J_3 and J_5 (131.44° vs 117.55° and 124.24°) (Table 1). J_5 is considerably weaker than J_3 although it has a larger ∠Ni−O−Ni angle, because the Ni3−O bond of the J_5 path is long (2.122 Å). That J_1 is FM is understandable because the ∠Ni−O−Ni angle is close to 90° (Table 1). J_2 strongly FM despite that its ∠Ni−O−Ni

(14) Greedan, J. E. *J. Mater. Chem.* **2001**, *11*, 37, and the references cited therein.
(15) Dai, D.; Whangbo, M.-H. *J. Chem. Phys.* **2004**, *121*, 672.
(16) Goodenough, J. B. *Magnetism and Chemical Bond*; Wiley: Cambridge, MA, 1963.

Table 3. Relative Energies (in meV per six FUs) of the Magnetic Ground States with the Spin Orientations Parallel and Perpendicular to the *c*-axis ($\|c$ and $\perp c$, respectively) in Terms of GGA+U+SOC Electronic Structure and MDD Interaction Calculations

	$\|c$	$\perp c$
GGA+U+SOC with U = 2.5 eV	0	−0.32
GGA+U+SOC with U = 4.5 eV	0	−0.25
MDD interaction	0	+0.45

angle deviates considerably from 90°. This is caused by the distortions of the $Ni2O_6$ and $Ni3O_6$ octahedra in the Ni2-$Ni3O_9$ dimer, in which the Ni^{2+} ions are pushed away from each other due to their Coulomb repulsion, so that the Ni−O bonds bridging the Ni2 and Ni3 atoms are lengthened while shortening the terminal Ni−O bonds (Figure 5a). As found for Na_3RuO_4,[17] the magnetic orbitals of the distorted $Ni2O_6$ and $Ni3O_6$ octahedra have smaller O 2p contributions from the O atoms of the long Ni−O bonds than from those of the short Ni−O bonds (Figure 5b,c).[18] In addition, the magnetic orbitals of $Ni2O_6$ differ mostly from those of $Ni3O_6$ in the locations of their large O 2p contributions on the three Ni2−O−Ni3 bridges (Figure 5b,c). When both magnetic orbitals have large O 2p orbital contributions on a same bridging O atom, these O 2p orbitals are nearly orthogonal to each other. Thus, the magnetic orbitals of $Ni2O_6$ overlap poorly with those of $Ni3O_6$. In general, a spin exchange J can be written as $J = J_F + J_{AF}$,[19,20] where J_F (> 0) and J_{AF} (< 0) is the FM and AFM components, respectively, and J_{AF} becomes negligible if the overlap integral between the magnetic orbitals is small. This explains why J_2 is strongly FM despite that the ∠Ni−O−Ni angle deviates considerably from 90°.

4. Effect of SOC and MDD Interactions on the Spin Orientation

In this section, we examine the spin orientation of Ni_3TeO_6 below T_N, which is found to be parallel to the *c*-axis by the neutron diffraction study.[5] To examine the cause for this orientation, we carry out GGA+U+SOC calculations for the magnetic ground state with the spin orientations parallel and perpendicular to the *c*-axis ($\|c$ and $\perp c$, respectively). These calculations reveal that the $\perp c$-spin orientation is more stable than the $\|c$-spin orientation (Table 3), in disagreement with experiment. Thus, we examine whether or not the experimentally observed spin orientation is caused by MDD interactions. In general, MDD interactions are weak, being of the order of 0.1 meV for two spin-1/2 ions separated by 2 Å,[21] and are often neglected in discussing the 3D magnetic order and the spin orientation of a magnetic solid. However, the 3D magnetic ordering of the strongly frustrated magnetic pyrochlore compounds $Dy_2Ti_2O_7$ and $Ho_2Ti_2O_7$, containing Ho^{3+} (f^{10}) and Dy^{3+}(f^9) ions, respectively, is explained in terms of MDD interactions.[22] For the spin orientation and 3D AFM ordering of $Sr_3Fe_2O_5$, containing high-spin Fe^{2+} (d^6) ions, MDD interactions were also found to be essential.[6] Therefore, we calculate the MDD interaction energies for the magnetic ground state (Figure 2d) of Ni_3TeO_6 with the $\|c$- and $\perp c$-spin orientations, as described in ref 6. To ensure that our results are converged with respect to the size of the cluster used for the summation of MDD interaction terms in eq 1, we included every two spin sites within the distance of 500 Å. These calculations reveal that the $\perp c$-spin orientation is less stable than the $\|c$-spin orientation (Table 3), in agreement with experiment. The energy difference between the $\|c$- and $\perp c$-spin orientations calculated from the MDD interactions is greater than that calculated from the GGA+U+SOC calculations. Consequently, the MDD interactions are responsible for the observed spin orientation in the magnetic ground state of Ni_3TeO_6.

5. Concluding Remarks

The spin exchanges J_1−J_5 of Ni_3TeO_6 extracted from the present GGA+U calculations correctly predict the observed magnetic structure below T_N, and lead practically to no spin frustration hence explaining why T_N and θ are nearly comparable in magnitude. The $\|c$-spin orientation observed in the magnetic structure below T_N is correctly predicted by MDD interactions, but not by SOC interactions. Thus, in discussing the 3D magnetic ordering and spin orientation of magnetic solids, it is important to consider the possibility of MDD interactions playing a critical role.

As found for Ni_3TeO_6,[5] a noncentrosymmetric magnetic solid is not necessarily ferroelectric below its 3D magnetic ordering temperature T_N if the ordered magnetic structure has no chirality. As recently found for $Ba_3NbFe_3Si_2O_{14}$,[23−25] however, a centrosymmetric magnetic solid becomes ferroelectric when its magnetic structure below its T_N is chiral. It should be noted that the loss of inversion symmetry, induced by a chiral magnetic ordering, allows the magnetic system to relax its charge distribution through SOC and become ferroelectric as a consequence.[26]

Acknowledgment. This work was supported by the Office of Basic Energy Sciences, Division of Materials Sciences, U.S. Department of Energy, under Grant DE-FG02-86ER45259, and also by the computing resources of the NERSC center and the HPC center of NCSU.

(17) Wu, F.; Kan, E. J.; Whangbo, M.-H. *Inorg. Chem.* **2010**, *49*, 3025.
(18) Our extended Hückel tight binding calculations were carried out by employing the SAMOA (Structure and Molecular Orbital Analyzer) program package (This program can be downloaded free of charge from the website, http://chvamw.chem.ncsu.edu/).
(19) Hay, P. J.; Thibeault, J. C.; Hoffmann, R. *J. Am. Chem. Soc.* **1975**, *97*, 4884.
(20) Whangbo, M.-H.; Koo, H.-J.; Dai, D. *J. Solid State Chem.* **2003**, *176*, 417.
(21) Ashcroft, N. W.; Mermin, N. D. *Solid State Physics*; Saunders College: Philadelphia; 1976; pp 673−674.
(22) Bramwell, S. T.; Gingras, M. J. P. *Science* **2001**, *294*, 1495, and the references cited therein.
(23) Marty, K.; Simonet, V.; Ballou, E. R.; Lejay, P.; Bordet, P. *Phys. Rev. Lett.* **2008**, *101*, 247201.
(24) Zhou, H. D.; Lumata, L. L.; Kuhns, P. L.; Reyes, A. P.; Choi, E. S.; Dalal, N. S.; Lu, J.; Jo, Y. J.; Balicas, L.; Brooks, J. S.; Wiebe, C. R. *Chem. Mater.* **2009**, *21*, 156.
(25) Lee, C.; Kan, E. J.; Xiang, H. J.; Whangbo, M.-H. *Chem. Mater.*, submitted for publication.
(26) Xiang, H. J.; Whangbo, M.-H. *Phys. Rev. Lett.* **2007**, *99*, 257203.